

Recovering quantum correlations in optical lattices from interaction quenches

Marek Gluza^{1,*} and Jens Eisert^{1,2,†}

¹*Dahlem Center for Complex Quantum Systems, Freie Universität Berlin, 14195 Berlin, Germany*

²*Helmholtz-Zentrum Berlin für Materialien und Energie, 14109 Berlin, Germany*

The atom gas microscope enables a level of inquiry into ultra-cold atoms in optical lattices unparalleled in any other quantum many-body system opening an exciting pathway towards understanding strongly interacting quantum systems. However, currently a direct measurement of a coherent current is out of reach. In this work, we show how to unify the two principal read-out techniques in optical lattice quantum simulators by using atom microscope measurements together with time-of-flight expansion into an optical superlattice. For this, we establish a data analysis method not resorting to the far-field approximation which reliably recovers the full covariance matrix, including off-diagonal correlations representing coherent currents. The signal processing builds upon semi-definite optimization, providing bona fide covariance matrices optimally matching the observed data. We demonstrate how the obtained information about non-commuting observables allows to lower bound entanglement at finite temperature which opens up the possibility to study quantum correlations in quantum simulations going beyond the capabilities of classical computers.

Quantum simulation experiments with ultra-cold atoms [1] have lead to numerous insights into the physics of strongly correlated quantum systems, both in static [2–5] and in dynamical [6–14] regimes. It is fair to say that there has been steady progress towards realizing the ambitious long-term goals set for quantum simulators [15]. Among them, the quest for understanding the precise mechanism underlying the physics of high- T_c superconductors may take a particularly important role, driving forward significant experimental progress on quantum simulations with *fermionic systems* [16–23]. In this line of research, achieving sufficiently cold temperatures is key and recently exciting progress has been reported, signified by an observation of very large anti-ferromagnets [16] with substantial evidence of string patterns [24]. Thanks to advances towards alleviating this particular bottleneck, it may in turn become a make or break issue to develop diagnostic tools regarding genuine *quantum correlations* in such systems. Specifically, one can anticipate that not only methods for identifying the presence of entanglement will be needed, this can be done via entanglement witnessing, but it will be instrumental to have ways of unambiguously answering the overall physical question of *how much entanglement* is there in a given quantum many-body system at finite temperature. Tools making this precise, providing certification in this sense [25], should then offer to understand the role of quantum mechanical effects on the conductance of systems that have so far evaded modelling using numerical calculations.

In this work, we set out to present diagnostic tools capable of tackling exactly these questions. They are based on information that is feasibly available via the so-called *atom gas microscope* [26–28]. Once this innovation had arrived, it allowed to observe string-order [3–5, 16], time-dependent features of ordered [2, 6–9, 13, 29] and disordered models [30]. It should be stressed that these observations would have been much more limited without the atom gas microscope, say us-

ing just time-of-flight type measurements. The atom microscope has a strong limitation, however, as at any given time it provides information only about the *local atom density*, which can be captured in terms of commuting operators in a quantum mechanical model. Because of that – possibly surprisingly – exploring *quantum correlations* in optical lattices is by far not straightforward.

In order to access expectation values of a set of non-commuting observables one must include some additional operations besides state preparation and direct measurements. Tomographic schemes employing measurements along a single quantization axis in conjunction with Bloch sphere rotations constitute the simplest example. In optical lattices, a sophisticated interference protocol [7] has been demonstrated to reveal entanglement, but it is applicable to only small systems. Exploiting known time evolution in conjunction with feasible measurements in recovery protocols in a general sense has been explored previously in Refs. [31–39].

As we will show here, observing the density at various times after an interaction quench into a super-lattice enables new insights: It allows to recover expectation values of non-commuting observables and *quantify entanglement* at finite temperature. This can give clues as to *why* a given system has a particular value of conductivity and what are the microscopic *mechanisms* at play in the quantum system studied. Put differently, understanding quantum correlations can allow for physical insights beyond the specific values of system parameters measured by linear-response. Linear-response measurements can be done both in quantum simulators and in materials. Concerning the latter, it has been possible to realize superconducting states at very high temperature. If this will be done in optical lattices then by our method or its possible extensions it will be possible to investigate the role of coherent quantum mechanical effects in the system. This is typically not possible in materials and in fact access to sophisticated quantum observables can become one of the most important strengths of quantum simulations in optical lattices [15].

Setting. The physical setting we have in mind is that of *fermionic atoms* in *optical lattices* [19, 20]. The discussion focuses on systems in one spatial dimension, but it should be clear that similar ideas carry over to higher-dimensional lat-

* marekgluza@zedat.fu-berlin.de

† jense@zedat.fu-berlin.de

tices. It is also worth pointing out that to an extent similar ideas have already proven highly useful and experimentally feasible in continuous quantum field settings provided by cold bosonic atoms trapped on an atom chip [31].

Notation-wise, we denote fermionic annihilation operators associated with some degree of freedom at lattice site x by \hat{f}_x . We put a focus on fermionic systems here but stress that the same machinery works similarly for bosons as well. The annihilation operators obey the canonical anti-commutation relations $\{\hat{f}_x, \hat{f}_y^\dagger\} = \hat{f}_x \hat{f}_y^\dagger + \hat{f}_y^\dagger \hat{f}_x = \delta_{x,y}$. The *covariance matrix* Γ of a state $\hat{\rho}$ is defined as the collection of second moments given by

$$\Gamma_{x,y} = \langle \hat{f}_x^\dagger \hat{f}_y \rangle_{\hat{\rho}} := \text{tr}[\hat{f}_x^\dagger \hat{f}_y \hat{\rho}] . \quad (1)$$

This matrix is in general a complex matrix $\Gamma \in \mathbb{C}^{L \times L}$, L being the system size¹. Additionally, we have $\Gamma = \Gamma^\dagger$ which means that it can be unitarily diagonalized by a Bogoliubov transformation of the type

$$\hat{p}_k = \sum_{x=1}^L U_{k,x}^* \hat{f}_x \quad (2)$$

such that $\tilde{\Gamma} = U \Gamma U^\dagger$ with $\tilde{\Gamma}_{k,k'} = \langle \hat{p}_k^\dagger \hat{p}_{k'} \rangle_{\hat{\rho}}$ is diagonal. Noting that $\hat{n}_k = \hat{p}_k^\dagger \hat{p}_k$ are the number operators of the eigen-modes \hat{p}_k we have that $\tilde{\Gamma} = \text{diag}(\lambda)$ has eigenvalues $0 \leq \lambda_k \leq 1$ by the Pauli principle. It is useful to write $A \succeq B$ if $A - B$ is a matrix with a non-negative spectrum which yields

$$0 \preceq \Gamma \preceq \mathbb{1} . \quad (3)$$

This is a convex constraint that will be included in our reconstructions using *semi-definite programming* methods [40]. Due to statistical noise, a direct estimate $\Gamma^{(\text{est})}$ of a covariance matrix Γ may not fulfill this constraint, but the recovery procedure should find a *physical* covariance matrix and hence taking into account Eq. (3) aids the reliability of the method.

A non-interacting fermionic (free) evolution conserving the particle number is generated by quadratic Hamiltonians

$$\hat{H}(h) = \sum_{x,y=1}^L h_{x,y} \hat{f}_x^\dagger \hat{f}_y \quad (4)$$

where $h = h^\dagger \in \mathbb{C}^{L \times L}$ is the coupling matrix. Most importantly, hopping on a line is captured by

$$\hat{H}_{\text{NN}} = \sum_{x=1}^{L-1} \hat{f}_x^\dagger \hat{f}_{x+1} + \text{h.c.} \quad (5)$$

where we use natural units in terms of the tunnelling time throughout the note. The Heisenberg evolution of mode operators reads

$$\hat{f}_x(t) = e^{it\hat{H}(h)} \hat{f}_x e^{-it\hat{H}(h)} = \sum_{y=1}^L G_{x,y}^*(t) \hat{f}_y \quad (6)$$

¹ If it was possible to directly measure currents then one would measure $\text{Re}[\Gamma_{x,y}] = \frac{1}{2} \langle \hat{f}_x^\dagger \hat{f}_y + \hat{f}_y^\dagger \hat{f}_x \rangle_{\hat{\rho}}$ and $\text{Im}[\Gamma_{x,y}] = -\frac{i}{2} \langle \hat{f}_x^\dagger \hat{f}_y - \hat{f}_y^\dagger \hat{f}_x \rangle_{\hat{\rho}}$ (the latter vanishes oftentimes given appropriate symmetries in the system).

where $G^*(t) = e^{-ith}$ is the *propagator* matrix which can be computed efficiently in the system size L .

Using (6) we see that the covariance matrix at time t is

$$\Gamma(t) = G(t) \Gamma(0) G(t)^\dagger . \quad (7)$$

The geometry of the lattice is encoded in the propagator G and by Eq. (7) is imprinted in the correlations. Our recovery method can be formulated independent of specifics of the lattice geometry. However, for clarity only, we shall apply it to the setting of most immediate practical interest, namely for a chain with open boundary conditions (5).

Tomographic read-out from interaction quenches. The core idea for reconstructing the covariance matrix Γ is the following protocol. The first step consists of preparing the state of interest:

$$(a) \text{ Prepare a fermionic state } \hat{\rho} . \quad (8)$$

Indeed, we do not have to know anything about how the state is prepared precisely, specifically, whether during the preparation there are non-trivial interactions between the particles or not. The preparation, provides a density matrix and we would like to reconstruct the second moments Γ of the possibly non-Gaussian state $\hat{\rho}$. In the second step, the task is:

$$(b) \text{ Double-up the lattice locally } \hat{f}_x \mapsto \hat{f}_{2x-1} . \quad (9)$$

In Fig. 1 we illustrate this by assuming that the system has initially been in a thermal state of Eq. (5) with a translationally invariant covariance matrix and a finite correlation length. We assume the doubling is fast and the *in-between* sites are still unoccupied while the correlations between the original sites have remained unchanged which gives rise to a distinct checker-board correlation pattern.

Next, we shall use coherent evolution under Eq. (5) to mix information about the coherent current into the particle number occupation operators:

$$(c) \text{ Quench to a free Hamiltonian } \hat{H}(h) . \quad (10)$$

This evolution will be a step that we can re-track in a computer simulation. In Fig. 1 we show results using \hat{H}_{NN} .

Finally, in the last step, we suitably exploit the existing read-out capabilities using the atom microscope which we assume to measure $\hat{N}_x = \hat{f}_x^\dagger \hat{f}_x$

$$(d) \text{ Measure } N_x(t) := \langle \hat{N}_x \rangle_{\hat{\rho}(t)} . \quad (11)$$

In this step, we find that we are indeed acquiring some information about currents thanks to the equation

$$N_x(t) = \Gamma_{x,x}(t) = \sum_{y,y'=1}^L G_{x,y}(t) G_{x,y'}^*(t) \Gamma_{y,y'}(0) . \quad (12)$$

We find that generically the right-hand side will depend on the off-diagonal matrix elements in the initial covariance matrix. The complete tomographic protocol consists of performing the steps (a-d) with $t = t_1, t_2, \dots, t_K$, where the time steps can be chosen to be equidistant.

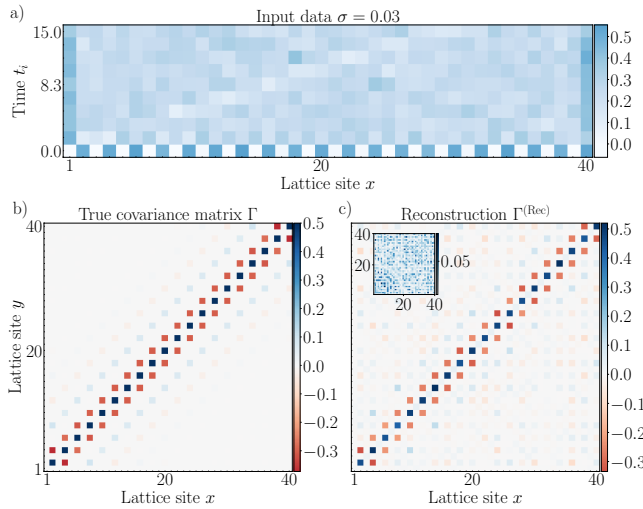


FIG. 1. Tomographic reconstruction. *a)* Input data for the reconstruction based on out-of-equilibrium data of local particle numbers $N_x(t_i)$ measured at K equidistant times after the quench to nearest-neighbour hopping in the superlattice. We model statistical fluctuations to be normally distributed due to a finite number $N_{\text{Shots}} \approx 10^4$ of accessible experimental runs yielding a representative value for the standard deviation $\sigma = 1/\sqrt{N_{\text{Shots}}/K} \approx 0.03$ of $N_x(t_i)$. *b)* The input data have been obtained by evolving a thermal covariance with inverse temperature $\beta = 3$. We have chosen a temperature so that there are relatively large currents to be recovered. The covariance matrix Γ is shown after step (b) after the sub-lattice has been created. Note that besides the new checker-board pattern, the correlations between sites are assumed to be exactly preserved. *c)* Results of the reconstruction $\Gamma^{(\text{Rec})}$. The extent of deviations shown in the inset is $\max |\Gamma_{x,y} - \Gamma_{x,y}^{(\text{Rec})}| \approx 0.1$ and is explained by the fact that among the data some $N_x(t_i)$ can be expected to fluctuate by about $\approx 3\sigma \approx 0.1$.

The reconstruction is based on an algorithm that in a nutshell takes a guess for the covariance matrix Γ' , evolves forward to the times t_i where the particle number data has been measured and checks whether the extrapolated distribution of the particles $N_x(t_i; \Gamma') = \Gamma'_{x,x}(t_i)$ reproduces the data $N_x(t_i; \Gamma') \approx N_x(t_i)$. In the next step an improved guess Γ'' is obtained such that the new observables $N_x(t_i; \Gamma'')$ are closer to the data

$$|N_x(t_i; \Gamma'') - N_x(t_i)| \leq |N_x(t_i; \Gamma') - N_x(t_i)|. \quad (13)$$

Formally, the algorithm solves the following optimization task. We collect all measured data into a vector b , and define a linear map \mathcal{A} which from an input covariance matrix Γ' produces the respective occupation numbers $N_x(t_i; \Gamma')$ in the same ordering as in b . The reconstruction $\Gamma^{(\text{Rec})}$ is an optimal solution to the optimization problem

$$\min_{0 \preceq \Gamma' \preceq 1} \|\mathcal{A}(\Gamma') - b\|_2. \quad (14)$$

The cost function is the 2-norm so we need to perform a least-square recovery problem with a positivity constraint [40]. Convexity of the problem guarantees an efficient convergence to a globally optimal solution with a polynomial runtime in the

system size L and desired accuracy $\epsilon > 0$ [40] and in practice takes a few seconds for $L \approx 40$. The results of the numerical reconstruction [41] employing a representative initial state to be recovered using our protocol is presented in Fig. 1. The particle number measurement need not be perfect and Fig. 1 discusses reconstructions that include statistical noise, too.

In step (a), additional assumptions can be included such as translation invariance in the initial state or a finite correlation length. The super-lattice trick (b) ensures that there will be visible non-equilibrium dynamics in the measurements. It hence circumvents the fact that if the quench Hamiltonian in (c) was translation invariant and the covariance matrix would happen to share this symmetry, then the evolution would be trivial which is related to the presence of local conservation laws [42]. That this is not the case is ensured precisely by quenching into a super-lattice [6, 43], but in principle any quench that leads to non-trivial dynamics (the covariance matrix is not a steady state of the quench Hamiltonian) can be considered. The reconstruction code [41] does not depend on the quench Hamiltonian (c) being nearest-neighbour, or whether there is a trap present so other variants are possible. If the couplings h are real, then the tomography reconstructs only the real part of the currents. This is enough for thermal states of quadratic Hamiltonians with no magnetic fields, see the appendix for reconstructions in their presence. Finally, note that similar ideas have successfully been applied in an atom chip experiment for a continuum system [31] where some unknown stray interactions have been present [44] but have been negligible in short time windows.

Quantum simulation studies of low-temperature systems in presence of Hubbard interactions with strength U are of particular interest. In experiments, the interactions will always be switched-off $U \rightarrow 0$ within a finite fraction of the tunnelling time. Crucially though, it follows directly from the Lieb-Robinson bound [45] that even if the quench has a finite duration then only the local correlations will be affected but, e.g., the presence of *long-range order* can be reliably inferred. If the quench has a negligible duration compared to the relevant time-scales in the system then even local correlations will be faithfully reconstructed implying the possibility of measuring also the *kinetic* energy in addition to the Hubbard interaction term that can be measured with the atom microscope. This would make it possible to perform in quantum simulators thermometry and calorimetry of Hubbard systems at low temperatures and hence will pave the way towards variational quantum simulation [46] in optical lattices.

Quantitatively estimating fermionic mode entanglement. Let us now show how to analyze the second moments Γ of a possibly interacting or non-equilibrium state to lower bound the so-called *entanglement cost* [47, 48]. This statement is particularly appealing as it goes beyond merely showing that there is entanglement present, but provides an answer to the question of ‘how much’ entanglement is there in the system [49–52]. The entanglement cost E_C quantifies mixed-state entanglement [47, 48] as it is the asymptotic rate at which maximally entangled pairs must be used for the creation of a given state $\hat{\rho}$ using local operations with classical communication (LOCC). E_C is broadly studied in quantum information

theory but is not easy to access in practice and therefore, especially in context of experiments, lower bounds by means of practically measurable quantities are needed.

We consider $\hat{\rho}$ to describe a bipartite system $A \cup B$, e.g., some number of sites in an optical lattice, and will explain how to lower bound $E_C(\hat{\rho})$. Firstly, if the asymptotically optimal creation of the state $\hat{\rho}$ via LOCC necessitates maximally entangled pairs at rate $E_C(\hat{\rho})$ then it could be that even more entangled pairs are needed for a system consisting of fermionic particles. Indeed, any physical operation in this case is subject to the fermionic parity and total number superselection rules (SSR) [53, 54] which further restrict LOCC. However, in Ref. [55] it has been shown that the asymptotic rates do not change, i.e., $E_C^{\text{SSR}}(\hat{\rho}) = E_C(\hat{\rho})$ (see the appendix). Secondly, we use that entanglement cost is lower bounded by distillable entanglement E_D

$$E_C(\hat{\rho}) \geq E_D(\hat{\rho}). \quad (15)$$

Thirdly, distillable entanglement is lower bounded by virtue of the *hashing bound* [56]

$$E_D(\hat{\rho}) \geq S(\hat{\rho}_A) - S(\hat{\rho}), \quad (16)$$

where for any state $\hat{\sigma}$ the von Neumann entropy is $S(\hat{\sigma}) = -\text{tr}[\hat{\sigma} \log_2(\hat{\sigma})]$ and the subscript in $\hat{\rho}_A$ indicates the reduction to subsystem A . Finally, the right hand side can be lower bounded by the same expression but now in terms of Gaussian entropies. Specifically, let us denote by $S^{(\Gamma)} = S(\hat{\rho}_\Gamma)$ to be the von Neumann entropy of a fermionic Gaussian state $\hat{\rho}_\Gamma$ with the same second moments Γ as $\hat{\rho}$. As shown in Refs. [57, 58] we have

$$S(\hat{\rho}_A) - S(\hat{\rho}) \geq S^{(\Gamma_A)} - S^{(\Gamma)} := E_G(\Gamma). \quad (17)$$

The Gaussian entropy $S^{(\Gamma)}$ can be easily computed from the recovered covariance matrix $\Gamma^{(\text{Rec})}$, see appendix for details. Summarizing, for any bipartite state $\hat{\rho}$ whose second moments Γ one can measure using our method we have found a lower bound to the entanglement cost $E_G(\Gamma) \leq E_C(\hat{\rho})$.

Entanglement cost at finite temperatures. We consider thermal states $\hat{\rho}_\beta = e^{-\beta \hat{H}_{\text{NN}}}/Z_\beta$, where Z_β is the partition function, β is the inverse temperature and $\Gamma^{(\beta)}$ is the corresponding covariance matrix. As detailed in the appendix without increasing E_C we can perform a *local* unitary Bogoliubov transformation in subsystems A and B individually. In Fig. 2a) we show the covariance matrix for $\beta = 3$ after such a local transformation showing that essentially two modes are non-trivially correlated. In Fig. 2b) we show the entanglement cost lower bound $E_G(\beta) \equiv E_G(\Gamma^{(\beta)})$ as a function of inverse temperature. We select either one or two modes in each subsystem and find a non-trivial lower bound $E_G(\beta) > 0$ for sufficiently low temperatures. Choosing one mode gives a non-trivial lower bound for higher temperatures than for two modes because the total entropy in the latter case tends to be larger at high temperature. In contrast, at extremely low temperatures, the one mode lower bound saturates at its maximum value $E_G^{(1+1)}(\beta) \leq 1$ while the two mode witness indicates that the entanglement cost of preparing $\hat{\rho}_\beta$ is asymptotically larger than that of one maximally entangled pair.

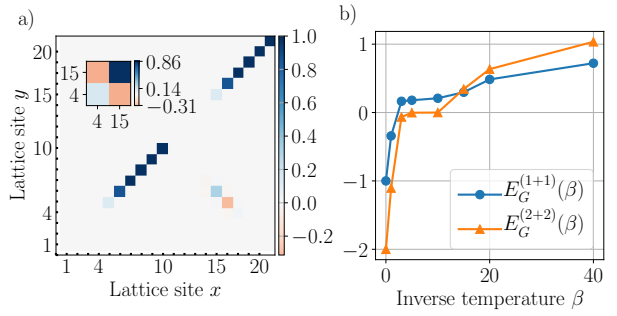


FIG. 2. **Entanglement cost at finite temperature.** a) Covariance matrix $\Gamma^{(D)} = U_D \Gamma^{(\beta)} U_D^\dagger$ for $\beta = 3$ after a local transformation $U_D = U_A \oplus U_B$. Two modes have distinct correlations, the inset shows the covariance matrix after selecting one mode in A and one mode in B which is used to compute $E_G^{(1+1)}(\beta)$. b) Selecting one mode in each subsystem gives a non-trivial entanglement cost lower for relatively large temperatures $E_G^{(1+1)}(\beta \approx 3) > 0$ while selecting 2 modes indicates larger values at low temperatures where large rates E_C may be required.

Going beyond the Gaussian case, note that the second moments of low-temperature states will vary continuously with the strength of the many-body interaction [59]. Thus we can be confident that a non-trivial E_C lower bound will be obtained for sufficiently weak interactions and low temperatures. Such states, e.g., in two spacial dimensions become difficult to treat numerically in practice, however, our reconstruction and entanglement quantification methods remain applicable for quantum simulation experiments.

Outlook. We have shown how to measure coherent currents in optical lattices by unifying atom microscope measurements with quenches into superlattices and performing reconstructions using semi-definite programming which does not resort to far-field approximations. We discuss in the appendix that the conceptual simplicity of our approach can allow to understand *systematic* limitations in an experimental implementation of steps (b) and (c). We remark, that our method does not depend on the geometry of the quench and instead of a superlattice other ways of inducing visible particle number dynamics can also be possible, e.g., simply expanding into a larger lattice. Our idea suggests further that lattice constrained time-of-flight dynamics may allow to increase the measurement precision, which is a surprising innovation of a technique as old as quantum mechanics.

Building on the accessibility of full covariance matrices, including coherent currents, we have put forward a novel entropic witness that allows to lower bound the entanglement cost. This is a quantitative measure of entanglement and is a stronger statement than merely showing its presence. We have shown that our witness can give non-trivial values at finite temperatures. This will remain true also for weak interactions as second moments should vary continuously in the strength of interactions. We hence, have established a method to recover and quantify quantum correlations in optical lattice quantum simulations which is applicable even in regimes where numerical calculations cease being practical.

Acknowledgements. We thank M. Greiner, C. Gross, P.

Preiss and R. Sweke for stimulating discussions. This work has been supported by the ERC (TAQ), the DFG (CRC 183, FOR 2724, EI 519/7-1), and the Templeton Foundation. This

work has also received funding from the European Unions Horizon2020 research and innovation programme under grant agreement No. 817482 (PASQuanS).

[1] I. Bloch, J. Dalibard, and S. Nascimbene, *Nature Phys.* **8**, 267 (2012).

[2] M. Greiner, I. Bloch, O. Mandel, T. W. Hänsch, and T. Esslinger, *Phys. Rev. Lett.* **87**, 160405 (2001).

[3] M. Endres, M. Cheneau, T. Fukuhara, C. Weitenberg, P. Schauss, C. Gross, L. Mazza, M. C. Banuls, L. Pollet, I. Bloch, and S. Kuhr, *Science* **334**, 200 (2011).

[4] M. E. Tai, A. Lukin, M. Rispoli, R. Schittko, T. Menke, D. Borgnia, P. M. Preiss, F. Grusdt, A. M. Kaufman, and M. Greiner, *Nature* **546**, 519 (2017).

[5] S. Trotzky, L. Pollet, F. Gerbier, U. Schnorrberger, I. Bloch, N. Prokof'ev, B. Svistunov, and M. Troyer, *Nature Phys.* **6**, 998 (2010).

[6] S. Trotzky, Y.-A. Chen, A. Flesch, I. P. McCulloch, U. Schollwöck, J. Eisert, and I. Bloch, *Nature Phys.* **8**, 325 (2012).

[7] A. M. Kaufman, M. E. Tai, A. Lukin, M. Rispoli, R. Schittko, P. M. Preiss, and M. Greiner, *Science* **353**, 794 (2016).

[8] S. Braun, M. Friesdorf, S. S. Hodgman, M. Schreiber, J. P. P. Ronzheimer, A. Riera, M. del Rey, I. Bloch, J. Eisert, and U. Schneider, *Proc. Natl. Ac. Sc.* **112**, 3641 (2015).

[9] J. P. Ronzheimer, M. Schreiber, S. Braun, S. S. Hodgman, S. Langer, I. P. McCulloch, F. Heidrich-Meisner, I. Bloch, and U. Schneider, *Phys. Rev. Lett.* **110**, 205301 (2013).

[10] S. Hofferberth, I. Lesanovsky, B. Fischer, T. Schumm, and J. Schmiedmayer, *Nature* **449**, 324 (2007).

[11] M. Gring, M. Kuhnert, T. Langen, T. Kitagawa, B. Rauer, M. Schreitl, I. Mazets, D. A. Smith, E. Demler, and J. Schmiedmayer, *Science* **337**, 1318 (2012).

[12] T. Langen, S. Erne, R. Geiger, B. Rauer, T. Schweigler, M. Kuhnert, W. Rohringer, I. E. Mazets, T. Gasenzer, and J. Schmiedmayer, *Science* **348**, 207 (2015).

[13] M. Cheneau, P. Barmettler, D. Poletti, M. Endres, P. Schauss, T. Fukuhara, C. Gross, I. Bloch, C. Kollath, and S. Kuhr, *Nature* **481**, 484 (2012).

[14] T. Schweigler, V. Kasper, S. Erne, I. E. Mazets, B. Rauer, F. Cataldini, T. Langen, T. Gasenzer, J. Berges, and J. Schmiedmayer, *Nature* **545**, 323 (2017).

[15] A. Acin, I. Bloch, H. Buhrman, T. Calarco, C. Eichler, J. Eisert, D. Esteve, N. Gisin, S. J. Glaser, F. Jelezko, S. Kuhr, M. Lewenstein, M. F. Riedel, P. O. Schmidt, R. Thew, A. Wallraff, I. Walmsley, and F. K. Wilhelm, *New J. Phys.* **20**, 080201 (2018).

[16] A. Mazurenko, C. S. Chiu, G. Ji, M. F. Parsons, M. Kanasz-Nagy, R. Schmidt, F. G. E., Demler, Greif, and M. Greiner, *Nature* **545**, 462 (2017).

[17] M. Köhl, H. Moritz, T. Stöferle, K. Günter, and T. Esslinger, *Phys. Rev. Lett.* **94**, 080403 (2005).

[18] T. Esslinger, *Ann. Rev. Con and Mat. Phys.* **1**, 129 (2010).

[19] U. Schneider, L. Hackermüller, J. P. Ronzheimer, S. Will, T. B. S. Braun, I. Bloch, E. Demler, S. Mandt, D. Rasch, and A. Rosch, *Nature Phys.* **8**, 213 (2012).

[20] T. Rom, T. Best, D. van Oosten, U. Schneider, S. Foelling, B. Paredes, and I. Bloch, *Nature* **444**, 733 (2006).

[21] C. S. Chiu, G. Ji, A. Mazurenko, D. Greif, and M. Greiner, *Phys. Rev. Lett.* **120**, 243201 (2018).

[22] A. Behrle, T. Harrison, J. Kombe, K. Gao, M. Link, J.-S. Bernier, C. Kollath, and M. Köhl, *Nature Phys.* **14**, 781 (2018).

[23] K. Viebahn, M. Sbroscia, E. Carter, J.-C. Yu, and U. Schneider, *Phys. Rev. Lett.* **122**, 110404 (2019).

[24] C. S. Chiu, G. Ji, A. Bohrdt, M. Xu, M. Knap, E. Demler, F. Grusdt, M. Greiner, and D. Greif, *Science* **365**, 251 (2019), <https://science.science.org/content/365/6450/251.full.pdf>.

[25] J. Eisert, D. Hangleiter, N. Walk, I. Roth, D. Markham, R. Parekh, U. Chabaud, and E. Kashefi, [arXiv:1910.06343](https://arxiv.org/abs/1910.06343) (2019).

[26] J. F. Sherson, C. Weitenberg, M. Endres, M. Cheneau, I. Bloch, and S. Kuhr, *Nature* **467**, 68 (2010).

[27] W. S. Bakr, A. Peng, M. E. Tai, R. Ma, J. Simon, J. I. Gillen, S. Fölling, L. Pollet, and M. Greiner, *Science* **329**, 547 (2010).

[28] C. Weitenberg, M. Endres, J. F. Sherson, M. Cheneau, P. Schauß, T. Fukuhara, I. Bloch, and S. Kuhr, *Nature* **471**, 319 (2011).

[29] J. Eisert, M. Friesdorf, and C. Gogolin, *Nature Phys.* **11**, 124 (2015).

[30] M. Schreiber, S. S. Hodgman, P. Bordia, H. P. Lüschen, M. H. Fischer, R. Vosk, E. Altman, U. Schneider, and I. Bloch, *Science* **349**, 842 (2015).

[31] M. Gluza, T. Schweigler, B. Rauer, C. Krumnow, J. Schmiedmayer, and J. Eisert, *Comm. Phys.* **3**, 12 (2020).

[32] M. Ohliger, V. Nesme, and J. Eisert, *New J. Phys.* **15**, 015024 (2013).

[33] S. T. Merkel, C. A. Riofrío, S. T. Flammia, and I. H. Deutsch, *Phys. Rev. A* **81**, 032126 (2010).

[34] A. Elben, B. Vermersch, M. Dalmonte, J. I. Cirac, and P. Zoller, *Phys. Rev. Lett.* **120**, 050406 (2018).

[35] P. Hauke, M. Lewenstein, and A. Eckardt, *Phys. Rev. Lett.* **113**, 045303 (2014).

[36] L. A. Pena Ardila, M. Heyl, and A. Eckardt, *Phys. Rev. Lett.* **121**, 260401 (2018).

[37] T. Qin, A. Schnell, K. Sengstock, C. Weitenberg, A. Eckardt, and W. Hofstetter, [arXiv preprint arXiv:1804.03200](https://arxiv.org/abs/1804.03200) (2018).

[38] M. Tarnowski, F. N. Ünal, N. Fläschner, B. S. Rem, A. Eckardt, K. Sengstock, and C. Weitenberg, [arXiv:1709.01046](https://arxiv.org/abs/1709.01046) (2017).

[39] S. Keßler and F. Marquardt, *Phys. Rev. A* **89**, 061601 (2014).

[40] S. Diamond and S. Boyd, *J. Mach. Learn. Res.* **17**, 1 (2016).

[41] M. Gluza, The numerical code is freely available at https://github.com/marekgluza/hopping_tomography and includes interactive Python notebooks allowing to reproduce the figures.

[42] M. Gluza, J. Eisert, and T. Farrelly, *SciPost Phys.* **7**, 38 (2019).

[43] M. Cramer, A. Flesch, I. McCulloch, U. Schollwöck, and J. Eisert, *Phys. Rev. Lett.* **101**, 063001 (2008).

[44] B. Rauer, S. Erne, T. Schweigler, F. Cataldini, M. Tajik, and J. Schmiedmayer, *Science* **360**, 307 (2018).

[45] E. H. Lieb and D. W. Robinson, *Commun. Math. Phys.* **28**, 251 (1972).

[46] C. Kokail, C. Maier, R. van Bijnen, T. Brydges, M. K. Joshi, P. Jurcevic, C. A. Muschik, P. Silvi, R. Blatt, C. F. Roos, *et al.*, *Nature* **569**, 355 (2019).

[47] C. H. Bennett, H. J. Bernstein, S. Popescu, and B. Schumacher, *Phys. Rev. A* **53**, 2046 (1996).

- [48] R. Horodecki, P. Horodecki, M. Horodecki, and K. Horodecki, Rev. Mod. Phys. **81**, 865 (2009).
- [49] J. Eisert, F. G. Brandao, and K. M. Audenaert, New J. Phys. **9** (2007).
- [50] K. M. R. Audenaert and M. B. Plenio, New J. Phys. **8**, 266 (2006).
- [51] O. Guehne, M. Reimpell, and R. F. Werner, Phys. Rev. Lett. **98**, 110502 (2007).
- [52] M. Cramer, A. Bernard, N. Fabbri, L. Fallani, C. Fort, S. Rosi, F. Caruso, M. Inguscio, and M. Plenio, Nature Comm. **4**, 3161 (2013).
- [53] J. Earman, Erkenntnis **69**, 377 (2008).
- [54] G. C. Wick, A. S. Wightman, and E. P. Wigner, Phys. Rev. **88**, 101 (1952).
- [55] N. Schuch, F. Verstraete, and J. I. Cirac, Phys. Rev. A **70**, 042310 (2004).
- [56] I. Devetak and A. Winter, Proc. R. Soc. Lon and A **461**, 207 (2005).
- [57] F. Pastawski, J. Eisert, and H. Wilming, Phys. Rev. Lett. **119**, 020501 (2017).
- [58] J. Eisert and M. W. Wolf, “Gaussian quantum channels,” in *Quantum Information with Continuous Variables of Atoms and Light* (Imperial College Press, London, 2007) pp. 23–42, arXiv:quant-ph/0505151.
- [59] C. V. Kraus and J. I. Cirac, New J. Phys. **12**, 113004 (2010).
- [60] M. Gluza, M. Kliesch, J. Eisert, and L. Aolita, Phys. Rev. Lett. **120**, 190501 (2018).
- [61] F. Arute, K. Arya, R. Babbush, D. Bacon, J. C. Bardin, R. Barends, S. Boixo, M. Broughton, B. B. Buckley, D. A. Buell, *et al.*, arXiv preprint arXiv:2004.04174 (2020).
- [62] S. T. Flammia and Y.-K. Liu, Phys. Rev. Lett. **106**, 230501 (2011).
- [63] M. A. Nielsen, Phys. Rev. Lett. **83**, 436 (1999).
- [64] J. Eisert and M. Cramer, Phys. Rev. A **72**, 042112 (2005).
- [65] N. Schuch, F. Verstraete, and J. I. Cirac, Phys. Rev. A **70**, 042310 (2004).
- [66] M. Gluza, C. Krumnow, M. Friesdorf, C. Gogolin, and J. Eisert, Phys. Rev. Lett. **117**, 190602 (2016).
- [67] M. M. Wolf, Phys. Rev. Lett. **96**, 010404 (2006).
- [68] I. Peschel, J. Stat. Mech. , P12005 (2004).

Appendix A: Symmetries of the Hamiltonian

Various symmetries of the Hamiltonian may lead to some aspects of the state to remain hidden in the tomographic recovery procedure, or more precisely some correlation functions may be unconstrained by the observed particle number dynamics. Such symmetries are discussed here. Some simple examples are the following.

(i) Hopping Hamiltonians mix correlations within the tunnelling correlation sector only. Therefore pairing correlations such as $\langle \hat{f}_x \hat{f}_y \rangle + \text{h.c.}$ can be arbitrary and their presence or absence does not modify the input to the tomographic recovery procedure.

(ii) If both the initial state and the quench Hamiltonian are translation invariant then even if there are non-trivial currents in the covariance matrix, the particle number dynamics remains unchanged. This can be seen by observing that both h and $\Gamma(0)$ can be simultaneously diagonalized by a Fourier transform and so their commutator vanishes at all times. This

implies that $N_x(t) = \Gamma_{x,x}(t) = \Gamma_{x,x}(0) = N_x(0)$ and the currents are unconstrained. We resolved this issue by doubling up the lattice which implies that every other site is unoccupied and necessarily the state is not translation invariant.

1. Zero magnetic fields

The case when the couplings h are real is related to the absence of magnetic fields. We will now show that if one quenches to a Hamiltonian with such couplings, then only the real part of the currents can be reconstructed. That is to say, let the state have some second moments $\Gamma = \Gamma^{(\text{Re})} + i\Gamma^{(\text{Im})}$ with $\Gamma^{(\text{Re})}, \Gamma^{(\text{Im})}$ being the real and imaginary parts, respectively. Then the tomography performed using the measurement of particle numbers will not constrain the imaginary part covariance matrix.

Let us now demonstrate that the particle number dynamics does not depend on the initial imaginary part of the currents if the couplings h are real. To see this, we note that $\Gamma^{(\text{Im})} = -\Gamma^{(\text{Im})T}$ because $\Gamma = \Gamma^\dagger$. Secondly, we will use that $h = h^T$ implies $G(t)^* = G(-t)$ and $G(t)^T = G(t)$. The particle numbers at time t are given by

$$N_x(t) = \Gamma_{xx}(t) = G(t)\Gamma^{(\text{Re})}G(t)^\dagger + iG(t)\Gamma^{(\text{Im})}G(t)^\dagger. \quad (\text{A1})$$

The first term related to the real part of the currents will in general influence the particle number dynamics. For the second term by transposing twice we see that

$$\begin{aligned} \Gamma^{(\text{Im})}(t) &:= G(t)\Gamma^{(\text{Im})}G(t)^\dagger & (\text{A2}) \\ &= \left(G(t)^*(\Gamma^{(\text{Im})})^T G(t)^T \right)^T \\ &= - \left(G(-t)\Gamma^{(\text{Im})}G(-t)^\dagger \right)^T \\ &= -\Gamma^{(\text{Im})}(-t)^T \end{aligned}$$

and

$$\begin{aligned} \Gamma^{(\text{Im})}(t)^* &= G(t)^*(\Gamma^{(\text{Im})})^*(G(t)^\dagger)^* & (\text{A3}) \\ &= G(-t)\Gamma^{(\text{Im})}G(-t)^\dagger \\ &= \Gamma^{(\text{Im})}(-t). \end{aligned}$$

The only way for the imaginary part of currents $\Gamma^{(\text{Im})}$ to contribute to particle number dynamics is via the diagonal matrix elements of its real part after the time evolution

$$\begin{aligned} \text{Re}[\Gamma^{(\text{Im})}(t)] &= \frac{1}{2}(\Gamma^{(\text{Im})}(t) + \Gamma^{(\text{Im})}(t)^*) & (\text{A4}) \\ &= \frac{1}{2}(\Gamma^{(\text{Im})}(t) - \Gamma^{(\text{Im})}(t)^T). \end{aligned}$$

The last relation proves that the real part of $\Gamma^{(\text{Im})}(t)$ is an antisymmetric matrix. This implies that its diagonal matrix elements are vanishing and hence the imaginary part of the

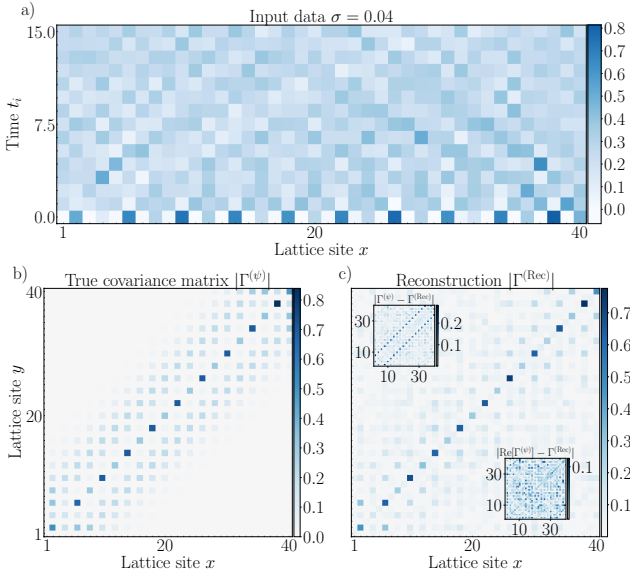


FIG. 3. **Reconstruction for quenched CDW.** *a)* The particle number dynamics used in the quench. *b)* The same covariance matrix as above is to be reconstructed. *c)* The reconstruction has not detected the presence of a complex-valued current. The upper inset shows that certain tunnelling correlation are missing, these precisely the imaginary part of the currents as shown in the bottom inset where the deviation is coming only from the random noise modelling finite statistical samples.

currents cannot be detected by the tomography after a quench to an evolution with real couplings so

$$\langle \hat{N}_x(t_i) \rangle_{\hat{\rho}_\Gamma} = \langle \hat{N}_x(t_i) \rangle_{\hat{\rho}_{\text{Re}[\Gamma]}}. \quad (\text{A5})$$

The next section discusses this property further in relation to practical examples.

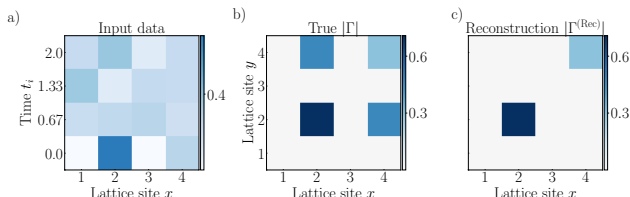


FIG. 4. **Tomographic recovery of two site system to a superlattice on 4 sites.** *a)* The particle number dynamics used as input as shown above does not depend on the complex part of the covariance matrix because we use the nearest-neighbour hopping Hamiltonian \hat{H}_{NN} with real couplings. *b)* The absolute value of the covariance matrix. The off-diagonal current is purely imaginary. *c)* As discussed the imaginary part of the covariance matrix is unconstrained and hence the reconstruction is missing the off-diagonal current. The evolution of the reconstructed covariance matrix yields particle numbers exactly matching the input as proven analytically.

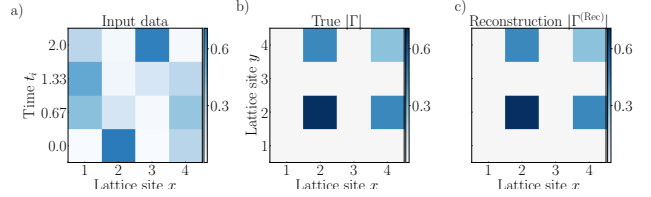


FIG. 5. **Recovery in presence of artificial magnetic fields.** *a)* The particle number dynamics is influenced by the complex part of the covariance matrix if we use a Hamiltonian $\hat{H} = \hat{H}_{\text{NN}} + i \sum_{x=1}^3 \hat{f}_x^\dagger \hat{f}_{x+1} + \text{h.c}$ with complex couplings. *b)* The same covariance matrix as above is to be reconstructed. *c)* The reconstruction now has detected the presence of the complex-valued current.

Appendix B: Strategies for experimentally benchmarking the systematics of the method on charge density waves

In Ref. [6] it has been shown how to prepare experimentally a charge density wave (CDW) which is just a Fock state vector with alternating particle occupation numbers $|\phi\rangle = |0, 1, 0, 1 \dots\rangle$ prepared on L sites and quench to free evolution. The covariance matrix of this state is then $\Gamma^{(\phi)} = \text{diag}(0, 1, 0, 1 \dots)$. Let us discuss that this state can be used to build trust in the reconstruction method.

First of all, we can make sure that the finite duration of the super-lattice creation when preparing the CDW does not induce correlations between sites, i.e., just using measurements using the atom microscope we can make sure that the covariance matrix is $\Gamma^{(\phi)} = \text{diag}(0, 1, 0, 1 \dots)$. This can be argued by a *fidelity witnessing* argument [60, 61]. If we have L sites and N_x does not deviate from 0 or 1 by more than ϵ , then the fidelity of the unknown state in the laboratory $\hat{\rho}_p$ with respect to the CDW Fock state vector $|\phi\rangle$ is lower bounded by

$$F(\hat{\rho}_p) = \langle \phi | \hat{\rho}_p | \phi \rangle \geq 1 - \varepsilon = 1 - \epsilon L, \quad (\text{B1})$$

where L as before is the number of lattice sites. Having said that, to benchmark our method it is not necessary to evaluate the fidelity to the full density matrix of $|\phi\rangle$ but it will suffice to bound the deviation in the experiment from the covariance matrix from $\Gamma^{(\phi)}$ using the Cauchy-Schwarz inequality

$$|\Gamma_{x,y}| \leq \sqrt{N_x N_y}, \quad (\text{B2})$$

which readily implies that $|\Gamma_{x,y}| \leq \sqrt{\epsilon}$ whenever $N_x \leq \epsilon$. If at a given site x the particle number is measured to be $N_x = 1 - \epsilon$ then after a Bogoliubov transformation swapping particles and holes we again obtain $|\Gamma_{x,y}| \leq \sqrt{\epsilon}$. We conclude that if the CDW preparation is extremely good and the atom microscope measurement, too, then just from this data one can conclude that there are *no* currents in the system with the strength of a quantum certification test [25, 62]. Such a certified Fock state with a precise bound on fidelity can be used as a starting point for benchmarking of the dynamics with or without interactions.

Note that the step of creating a state with no currents can be verified by the static information about particle numbers alone using the atom microscope. Once we know that there

is no currents in the initial state, then we can create them by known dynamics. If this is done and the dynamics can be simulated numerically then one obtains an experimental state with well-grounded prior knowledge what currents to expect to be present in the system and one can verify the functioning of the tomographic reconstruction. The next section shows an example where we present results for reconstructions of time-evolved CDW states.

Check #1: Reconstructing a known current assuming \hat{H}_{NN}

Assuming the Hamiltonian is \hat{H}_{NN} we can consider some fixed time t_0 and attempt to reconstruct the state vector

$$|\psi\rangle = e^{-it_0\hat{H}_{\text{NN}}} |\phi\rangle \quad (\text{B3})$$

which has the covariance matrix $\Gamma^{(\psi)} = G(t_0)\Gamma^{(\phi)}G(t_0)^\dagger$. If we assume the free nearest-neighbour hopping evolution to be exact, then we can be sure that the covariance matrix in the laboratory is ϵ -close to $\Gamma^{(\psi)}$ if we verified that the experimental preparation of the CDW has been ϵ -close to $\Gamma^{(\phi)}$. But then knowing that, we know precisely which off-diagonal currents should be reconstructed.

The check reads: One prepares a CDW and performs quenches to times $t = t_0, t_0 + \Delta t, \dots, t_0 + T$ equi-distributed in steps Δt . From the measured data, one recovers the covariance matrix assuming that the data have been taken at times $t = 0, \Delta t, \dots, T$. The tomography should return a covariance matrix close to $\Gamma^{(\psi)}$. Note that when running the tomography here we are bypassing the step (b) from the main text. We can learn from the atom microscope measurements in step (d) whether the initial state has indeed been prepared with high fidelity. And it is not necessary to double up the lattice anymore as the initial state is not translation invariant by construction. Having said that, the super-lattice creation is going to be important when studying homogeneous thermal states that will be of interest in future quantum simulation experiments and hence it is important to map out the systematic influence of this step on the tomography which we describe next.

Check #2: Assessing the systematic influence of doubling up the lattice

The above check tests the reconstruction of a state with known currents but with the input influenced by statistical errors. In the check the steps (b-d) have been on purpose bypassed as much as possible. The lattice doubling has been employed only in the sense of the state preparation in step (a).

It is possible to check how step (b) influences the reconstruction in the experiment. Again the task is to prepare the CDW with covariance matrix $\Gamma^{(\phi)}$ and evolve it under the nearest-neighbour hopping Hamiltonian of L sites to time t_0 obtaining the covariance matrix $\Gamma^{(\psi)}$. Then the super-lattice from step (b) should be created resulting in the checkerboard covariance matrix $\Gamma^{(\psi,b)}$. In step (c) the system should be evolved under the nearest-neighbour hopping Hamiltonian

(now on the doubled lattice) to times $t = 0, \Delta t, \dots, T$. As always in the last step (d) local particle numbers at each of the times are to be estimated to obtain the input to the reconstruction.

The results for the tomographic recovery in this scenario with $t_0 = 1$ are shown in Fig. 3. The input is depicted in Fig. 3a) after being subjected to noise modelling statistical errors. Note that the system considered here is far from being in thermal equilibrium and the particle numbers are changing over time-scales that are longer than those considered in the scenario discussed in the main text where the system was closer to thermal equilibrium. The checker-board covariance matrix $\Gamma^{(\psi,b)}$ is shown in Fig. 3b). In Fig. 3c) we show the results of the reconstruction. Importantly, the reconstruction does not recover the true covariance matrix as shown in the upper inset of Fig. 3c). As explained above, this is because this reflects a non-equilibrium situation with a non-trivial imaginary part of currents $\text{Im}[\Gamma^{(\psi,b)}] \neq 0$. On the other hand, as shown in the lower inset of Fig. 3c) the output of the reconstruction closely matches the real part of currents $\text{Re}[\Gamma^{(\psi,b)}]$. In fact, these are reliably recovered as they influence non-trivially the dynamics of the particle number and the deviations stem from the random noise realization that has been added to the input and is shown in Fig. 3a).

Check #3: Benchmarking the reconstructions in the presence of artificial magnetic fields

In this last section we show how to check the method experimentally if one wishes to reconstruct also the imaginary part of the currents. For this, it is necessary to have complex tunnelling amplitudes present during the tomographic quench in step (c). There does not seem to be a canonical choice which model to choose as this depends on the way the optical lattice is modulated in order to obtain the artificial magnetic field. We hence show a minimal example where the initial system is a two-site optical lattice with a single particle. Again we perform an evolution with $t_0 = 1$ which leads to a single tunnelling current $\Gamma_{1,2} \neq 0$ which turns out to be purely complex in this case. We then double up the lattice obtaining 4 sites and as above the particle numbers are to be measured after evolutions in the superlattice at equidistant times.

Fig. 4 shows that again simple hopping evolution does not uncover anything about the complex current. In contrast Fig. 5 shows that adding a simple complex hopping amplitude to the quench Hamiltonian in step (c) leads to a full reconstruction of the current. In both examples we did not add noise on the particle numbers so that the difference in the dynamics can be more easily compared between the evolution with and without the magnetic fields.

Summarizing this check, we point out that if it was possible to reconstruct using some Hamiltonian which has real couplings $\hat{H}_{(c),\text{real}}$ and additionally using a Hamiltonian that adds imaginary couplings without modifying the previous ones $\hat{H}_{(c),\text{general}} = \hat{H}_{(c),\text{real}} + \hat{H}_{(c),\text{imag}}$ then one can do two series of data taking and the tomography using $\hat{H}_{(c),\text{general}}$ should give a similar real part of the covariance matrix to that

obtained using $\hat{H}_{(\text{c}),\text{real}}$.

Appendix C: Fermionic mode entanglement

In this section, we provide further insights into the operational meaning of the entanglement quantified based on our reconstructions, and what *fermionic mode entanglement* operationally means. We denote the fermionic Fock state vectors by

$$|\mu\rangle_F := (\hat{f}_1^\dagger)^{\mu_1} \dots (\hat{f}_L^\dagger)^{\mu_L} |\emptyset\rangle \quad (\text{C1})$$

with $\mu \in \{0, 1\}^{\times L}$ and where $|\emptyset\rangle$ denotes the vacuum state vector defined as satisfying $\hat{f}_x |\emptyset\rangle = 0$ for all $x = 1, \dots, L$. For a given order (so basically a symmetric group element $S \in S_L$ that captures the order of the fermionic modes when mapping them to spins), we can define a Jordan-Wigner transformation by the relations

$$\hat{f}_x = Z^{\otimes x-1} \otimes \begin{pmatrix} 0 & 1 \\ 0 & 0 \end{pmatrix} \otimes \mathbb{1}_2^{\otimes L-x} \quad (\text{C2})$$

with

$$Z = \begin{pmatrix} 1 & 0 \\ 0 & -1 \end{pmatrix} \quad (\text{C3})$$

referring to the Pauli- z matrix. This choice of the Pauli- z matrix fixes its eigenbasis so that we have the convention $Z |\nu\rangle_S = (-1)^\nu |\nu\rangle_S$ with $\nu = 0, 1$ and then Eq. (C2) imply directly that

$$|\mu\rangle_F = \otimes_{x=1}^L |\mu_x\rangle_S. \quad (\text{C4})$$

Note that any ordering of modes can give rise to such a qubit representation where fermionic operators and state vectors can be expressed in an explicit matrix form, but once chosen it should remain fixed throughout calculations. Importantly, occupation states of modes after a non-trivial Bogoliubov transformation will not anymore have such a tensor-product form and one should consider the decomposition into antisymmetric subspaces.

Having fixed the reference ordering of modes, we have a natural notion of fermionic subsystems: A subsystem A consists of a collection of modes, i.e., positions in the lattice, while B is constituted by the complementing modes. In all what follows, we are perfectly free to take the ordering so that modes labeled $1, \dots, |A|$ give rise to subsystem A , while $|A| + 1, \dots, L$ give rise to B .

We now turn to quantum states in such a fermionic setting. Given a quantum state $\hat{\rho}$ supported on the Hilbert space of the entire system, the reduced state $\hat{\rho}_A$ is defined via functionals of observable algebras: Specifically, it will reflect correlation functions involving operators acting in A equal to those of the global state. That is to say, in what follows, we can treat the system as a system of $|A|$ qubits held by A and $L - |A|$ qubits held by B .

Any allowed quantum operation performed within an isolated fermionic system must respect the *parity of fermion*

number super-selection rule [53, 54], which implies that at any time, any correlation function involving an odd number of fermionic creation and annihilation operators must vanish. This means that if one performs operations and measurements locally in subsystems A and B , then to describe any of such processes it suffices to consider the reduced states $\hat{\rho}_A$ and $\hat{\rho}_B$ to be a direct sum of sectors reflecting even and odd particle numbers in A and B , respectively. That is to say, we can first make use of a projection $\pi \otimes \pi$ which projects each of the local subsystems A and B into a direct sum of even and odd particle numbers.

Local operations with classical communication reflecting super-selection rules, referred to as LOCC+SSR, can hence be identified with local operations in the qubit systems reflecting A and B under the Jordan-Wigner transformations, respecting the local direct sum structure of even and odd particle numbers in A and B and the total system. This is a perfectly operational prescription. We call a quantum state *mode entangled* throughout this article, if it is not a convex combination of uncorrelated quantum states in fermionic modes.

Appendix D: Single copy fermionic mode entanglement

There is a subtlety arising in the fermionic context, however: This has to do with the presence of super-selection rules. This can be seen as follows. Turning to quantitative prescriptions, one can define *single-copy entanglement* [63, 64] as the maximum probability at which one can – at least in principle – extract maximally entangled states of distinguishable quantum systems out of the original system of fermionic modes, making use of any operation in LOCC+SSR that is allowed by quantum mechanics. In this prescription, one may make use of suitable physical interactions or measurements respecting LOCC+SSR. The target distinguishable quantum systems can either be seen as being actually available in the laboratory, e.g., as spin degrees of freedom, or as a conceptual tool to precisely think of mode entanglement in the first place.

Interestingly, in this sense, a state $\hat{\rho} = |\psi\rangle\langle\psi|$ with $|\psi\rangle = (|0, 1\rangle_F + |1, 0\rangle_F)/\sqrt{2}$ represented as

$$|\Phi\rangle := \frac{1}{\sqrt{2}}(|0\rangle_S \otimes |1\rangle_S + |1\rangle_S \otimes |0\rangle_S) \quad (\text{D1})$$

is not *single-copy entangled*, as no physically allowed protocol can map this state onto an entangled state of distinguishable quantum systems with any non-zero probability. The projection π acting as

$$|\Phi\rangle\langle\Phi| \mapsto (\pi \otimes \pi)|\Phi\rangle\langle\Phi|(\pi \otimes \pi) \quad (\text{D2})$$

will render the state operationally indistinguishable from a quantum state that is merely classically correlated and contains no quantum entanglement. That is to say, for all practical purposes, the state does not contain any entanglement that can be operationally extracted (i.e., with all operations allowed) from a single specimen or copy. It is important to stress that this statement is referring to single-copy entanglement only: It is perfectly an entangled state if asymptotic state transformations are being allowed for, as explained below.

Appendix E: Distillable fermionic mode entanglement and asymptotic state manipulation

However, the above fermionic two-mode quantum state represented by the state vector $|\psi\rangle = (|0,1\rangle_F + |1,0\rangle_F)/\sqrt{2}$ is in fact *many-copy entangled*, as the SSR is asymptotically not detrimental to the entanglement content of the state vector. Such asymptotic notions involving *many copies of identically prepared systems* at the same time are the most commonly applied standard notions of entanglement theory, much inspired by notions of classical information theory. Here, one still restricts to quantum operations local to A and B , coordinated by classical means by communicating measurement outcomes between A and B . But one assumes to have available several copies (or specimens) of the quantum many-body systems available and is allowed to coherently manipulate the quantum state over the copies. Obviously, in practical settings, it is implausible to achieve completely general operations of this kind: It is still a highly convenient abstraction.

The notion of the *distillable entanglement* [47, 48] captures most naturally the resource character of entanglement in quantum information theory. It is in a way the 'entanglement content' of a state. It is defined as the optimal rate at which one could extract maximally entangled pairs of distinguishable systems in such a hypothetical optimal state manipulation from many identical copies. This notion not only allows to detect the presence of fermionic entanglement: It also allows to make *quantitative estimates*, which is precisely what we are interested in here. More precisely and specifically put, the distillable entanglement quantifies the asymptotic rate at which one can extract ('distill') distinguishable approximately perfect maximally entangled qubit pairs ('Bell pairs') as in Eq. (D1) of distinguishable quantum systems from many identical copies of an input state composed of fermionic modes, using quantum operations from LOCC+SSR [65]. For a fermionic initial quantum state $\hat{\rho}$ on L modes partitioned into A and B , the entanglement distillation problem involves as initial state the bona fide quantum state of n copies on nL modes. The final state is asymptotically in n better and better approximating m copies of a maximally entangled pure quantum state associated with the state vector

$$|\psi_{\text{Final}}\rangle = |\Phi\rangle^{\otimes m}, \quad (\text{E1})$$

in trace-norm $\|\cdot\|_1$, so will approximate m Bell pairs. The larger m is, the larger is the yield of this procedure. The distillable entanglement under LOCC+SSR is now

$$E_D^{\text{SSR}}(\hat{\rho}) = \limsup_{n \rightarrow \infty} \frac{n}{m}, \quad (\text{E2})$$

as the supremum over all LOCC+SSR protocols for n input copies and m output copies each. Since the super-selection rule is asymptotically not altering the rate, we have that

$$E_D^{\text{SSR}}(\hat{\rho}) = E_D(\hat{\rho}), \quad (\text{E3})$$

where the right hand side is the distillable entanglement for the spin equivalent of $\hat{\rho}$, possibly not respecting super-selection rules [65]. The right hand side can be bounded from

below by the *hashing bound*, as stated in the main text. The *entanglement cost* E_C refers to the optimal rate that can be achieved in the converse, starting from m copies of maximally entangled Bell pairs and achieving approximately perfect n copies of the anticipated target state. Again,

$$E_C^{\text{SSR}}(\hat{\rho}) = E_C(\hat{\rho}), \quad (\text{E4})$$

while in general $E_C(\hat{\rho}) \geq E_D(\hat{\rho})$, as the process of distillation can be lossy compared to the process of formation that the entanglement cost captures.

Appendix F: Evaluation of the witness

We present details on how to evaluate the entanglement witness $E_G(\Gamma)$ in this section. We shall make use of the fact that the *von Neumann entropy*, in general being defined for a quantum state as

$$S(\hat{\rho}) = -\text{tr}[\hat{\rho} \log(\hat{\rho})], \quad (\text{F1})$$

is unitarily invariant. For this reason, it can be easily and efficiently be evaluated for a fermionic Gaussian state. In the main text we are using the fact that given the covariance matrix $\Gamma = \Gamma(\hat{\rho})$ of the state $\hat{\rho}$, we can associate to the state a unique Gaussian state $\hat{\rho}^{(\Gamma)}$ with the same second moments. In fact, we have

$$\hat{\rho}^{(\Gamma)} = \text{argmax}_{\hat{\sigma}} \{S(\hat{\sigma}) \text{ s.t. } \Gamma(\hat{\sigma}) = \Gamma(\hat{\rho})\}, \quad (\text{F2})$$

which means that Gaussian states give rise to the maximum possible von Neumann entropy, among all quantum states for fixed second moments Γ [66].

For thermal states of particle number preserving Hamiltonians and for limits of such finite-temperature states, the entropy of a Gaussian state can be computed from the covariance matrix using standard expressions, see, e.g., Refs. [67, 68], by obtaining the vector n of the eigenvalues of Γ . We then have

$$S^{(\Gamma)} = S(\hat{\rho}^{(\Gamma)}) = -\sum_{k=1}^L f(n_k), \quad (\text{F3})$$

where the function $f : [0, 1] \rightarrow [0, 1]$ is defined as

$$f(x) = \begin{cases} -x \log(x) - (1-x) \log(1-x), & \text{if } x > 0, \\ 0, & \text{if } x = 0. \end{cases} \quad (\text{F4})$$

This formula can be evaluated efficiently in the number of modes. Finally, let us remark that the second moments of a *reduced* density matrix $\hat{\rho}_A$ describing a subsystem A is obtained by restricting the second moments to A which yields the corresponding covariance matrix Γ_A and hence for a Gaussian state

$$S(\hat{\rho}_A) = S^{(\Gamma_A)}, \quad (\text{F5})$$

as an expression in terms of the covariance matrix.

Appendix G: Optimizing the witness value via local Bogoliubov transformations

Our goal is to maximize the witness at hand to achieve the tightest possible lower bound bound. In the main text we gave an example where system A consists of the first 10 modes $A = \{1, 2, \dots, 10\}$ and $B = \{11, \dots, 20\}$. If we would apply the witness directly to systems A and B then it will give non-trivial values only for lowest temperatures where the thermal state is very close to the ground state. Indeed, in the case if the global quantum state is pure, then we have $E_G(\Gamma) = S^{(\Gamma_A)} - S^{(\Gamma)} \approx S^{(\Gamma_A)}$ and whenever the ground state is effectively described by a conformal field theory the subsystem entropy will scale logarithmically in the size of A . In the other limit of large temperatures, the entropies of whole system and subsystem A will both scale according to the volume and so the witness will have a negative value. To fix this, one has to make use of the freedom to make local unitary rotations on each subsystem. The goal here is to find some modes that carry only very little entropy such that the witness has a chance to be non-negative.

In general finding the optimal local unitaries that maximize the witness can be complicated but we found that the following heuristic is helpful. Denote by Γ_A and Γ_B the principal sub-matrices of Γ which are the covariance matrices of subsystems A and B and let U_A and U_B be the corresponding

diagonalization unitaries. Then the Gaussian state $\hat{\rho}'$ with the second moments given by

$$\Gamma' = U \Gamma U^\dagger = \begin{pmatrix} \Lambda_A Q_{A,B} \\ Q_{A,B}^\dagger \Lambda_B \end{pmatrix} \quad (G1)$$

where $U = U_A \oplus U_B$, features an identical amount of entanglement because the entanglement cost is invariant under local unitary transformations $E_C(\hat{\rho}) = E_C(\hat{\rho}')$. We hence can focus on the quantum state $\hat{\rho}'$.

We observe that this is a viable *distillation* heuristic, as now there can be a mode $a \in A$ and a mode $b \in B$ such that their covariance matrix $\Gamma'_{\{a,b\}}$ features a larger purity than before. This is the meaning of the sparse off-diagonal structure seen in the figure presented in the main text. We can restrict to these modes because entanglement cost is monotonous under partial traces

$$E_C(\hat{\rho}') \geq E_C(\hat{\rho}'_{a,b}), \quad (G2)$$

i.e., discarding some degrees of freedom can only decrease the available entanglement resources. This discarding however is crucial because we get a better chance for the witness value to be non-trivial – for this the discarded modes should take away most of the entropy while the reduced state of the remaining modes should be as pure as possible.